# Molecular Insight into Microstructural and Dynamical Heterogeneities in Magnesium Ionic Liquid Electrolytes

Long Su, Xinpei Gao,* Alessandro Mariani, Xu Liu, Stefano Passerini, Yanan Gao, and Liqiang Zheng*

**ABSTRACT:** Ionic liquids (ILs) are promising designer solvents for multivalent electrolytes, enabling the modulation of molecular-level interactions of solvate species. The molecular mechanism of multivalent-ion clustering and its impact on electrolytes properties is far less studied than that of ion pairs. Herein, we explore the effect of ion clusters on the transport and electrochemical behavior of IL-based electrolytes for Mg batteries. Simulation and small-angle X-ray scattering results indicate that ILs with higher denticity effectively suppress ion agglomeration and parasitic reactions of the Mg electrolytes. Although ion clustering reduces the diffusivity of $Mg^{2+}$, the Coulombic efficiency for the reversible Mg deposition/stripping process is improved, highlighting the importance of microstructural and dynamical heterogeneities in the rational design of enhanced multivalent electrolytes.

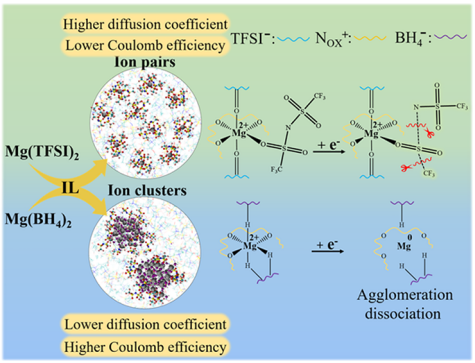


Ionic liquids (ILs), are promising nonmolecular solvents composed solely of ions, differing from water and organic solvents. ILs are nonvolatile and nonflammable, possessing high thermal stability, good conductivity, and wide electrochemical stability window.[1−3] These unique properties make ILs ideal components of electrolytes offering improved performance and safety for rechargeable multivalent batteries.[4−6]

Historically, ILs have been deemed to share similarities with molecular liquids or salt solutions as homogeneous, coherent, and isotropic liquids. However, it is known since 2006 that ILs are structurally[7] and dynamically[8] heterogeneous. Since then, ILs have been increasingly reported as structured solvents, demonstrating microstructural heterogeneity features ranging from supramolecular to mesoscopic hierarchical structures.[9−11] Intra- and interionic interactions give rise to various short-range ordering structures including ion pairs, clusters, and result in noticeable mesoscopic agglomeration in ILs, which influence the dynamical properties of IL-based electrolytes. Therefore, a thorough understanding of the formation of heterogeneous microstructures in IL-based electrolytes is essential for the rational design of optimized multivalent electrolytes. To date, both experimental techniques and theoretical calculations have provided exhaustive insights into structural features of ion pairs in IL-based electrolytes.[12−15] However, the molecular mechanism of ion cluster and its impact on electrolytes properties is far less studied than that of ion pairs. Representative studies on agglomeration rates, stability, and transport behavior of ion clusters have been reported for organic electrolytes.[16−18] Despite such studies on transport properties of solvated clusters in organic solvent, a comprehensive description of ion clusters in IL-based electrolytes is still in the infancy stage and requires further research to expand our understanding of ion agglomeration effect on dynamical as well as electrochemical behavior of IL-based electrolytes.

Given the complicated components of IL-based electrolytes, it is often difficult to experimentally investigate the structural and electrochemical behavior of ion clusters under working conditions. For instance, although we already achieved precise control of ion speciation in IL-based electrolytes to facilitate reversible Mg and Ca deposition/stripping process, it is still unclear whether the electroactive ion speciation appears in ion pairs or ion clusters from spectroscopy analysis of the IL-based electrolytes.[19,20] Herein, we report the effect of ion clusters on transport and electrochemical behavior of IL-based Mg electrolytes. Large-scale classical molecular dynamics (CMD) simulations and ab initio molecular dynamics (AIMD) simulations were conducted to reveal solvation, clustering, transport behavior, and deposition paths of the electrolytes. These properties were examined across two simple Mg salts ($MgTFSI_2$ and $Mg(BH_4)_2$) and four different alkoxy-functionalized ILs ($N_{OX}TFSI$, $x$ = 1, 3, 5, 7, as shown in Figure 1a). In designing IL-based electrolytes, the molar ratio of Mg salts to ILs is constant at 1:4 to highlight the electroactive ion speciation differences.[21]

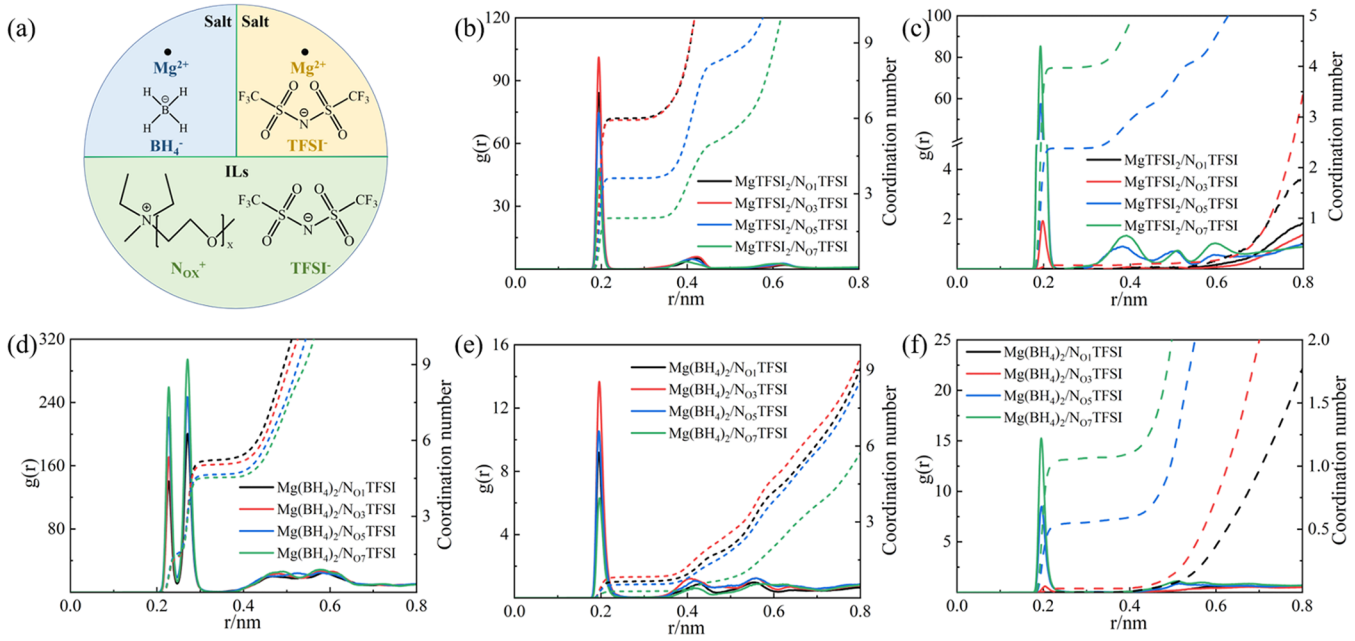


**Figure 1.** (a) Chemical structure and abbreviation of component ions of salts and ILs. RDF (solid line) and coordination number (dotted line) profiles of (b) $Mg^{2+}$−O(TFSI ), and (c) $Mg^{2+}$−O($N_{OX}^{+}$) in $MgTFSI_2$/IL electrolyte and (d) $Mg^{2+}$−B($BH_4$ ), (e) $Mg^{2+}$−O(TFSI ), and (f) $Mg^{2+}$−O($N_{OX}^{+}$) in $Mg(BH_4)_2$/IL electrolyte.

We first analyzed the coordination structures of $Mg^{2+}$ in both $MgTFSI_2$/IL and $Mg(BH_4)_2$/IL electrolyte. As seen in parts b and c of Figure 1, the radial distribution functions (RDFs) between $Mg^{2+}$ and O($TFSI^-$) and that between $Mg^{2+}$ and O($N_{OX}^{+}$) in all systems show sharp peaks at approximately 2.0 Å, corresponding to a total coordination number of $Mg^{2+}$−O of about 6, indicating the $Mg^{2+}$ is 6-fold coordinated by oxygen atoms from $TFSI^-$ or $N_{OX}^{+}$ in $MgTFSI_2$/IL electrolyte.[22,23] Intuitively, the coordination structures of $Mg^{2+}$ vary considerably as a function of the studied ILs solvent. Figure S1 shows the representative post equilibrium simulation snapshots of various $MgTFSI_2$/IL electrolyte. In the solvents with the short alkoxy chain cation, $N_{O1}$TFSI and $N_{O3}$TFSI, $TFSI^-$ fill the first solvation shell without the appearance of the $N_{O1}^{+}$ or $N_{O3}^{+}$ cation, which is supported by experimental results obtained by Raman spectra measurements in our previous work.[21] Subsequently, it is evident that the number of coordinated $TFSI^-$ in the first solvation shell is reduced, and the number of coordinated $N_{OX}^{+}$ is enhanced, as the cation chain length grows to $N_{O5}^{+}$ and $N_{O7}^{+}$. Comparative analysis indicates that the longer alkoxy chain of $N_{OX}^{+}$ possesses stronger coordination ability than $TFSI^-$, as judged by the more effective displacement of $TFSI^-$ from the $Mg^{2+}$ first solvation shell. The coordination structure is displayed in Figure S2a, which shows the proportion of $Mg^{2+}$ in which zero to six coordinated oxygen atoms belong to $TFSI^-$. Hence, the difference in the proportion of $Mg^{2+}$ as well as the RDFs indicate that the cation changes the $Mg^{2+}$ coordination structure. Almost all $Mg^{2+}$ coordinate exclusively to $TFSI^-$ to form $Mg^{2+}$−$TFSI^-$ ion pairs in $MgTFSI_2/N_{O1}$TFSI and $MgTFSI_2/N_{O3}$TFSI electrolyte. On the contrary, in the $MgTFSI_2/N_{O5}$TFSI and $MgTFSI_2/N_{O7}$TFSI electrolyte, dominant $Mg^{2+}$ tends to be coordinated with three and two oxygen atoms belonging to $TFSI^-$, respectively. The coordination structure of five oxygen atoms belonging to $TFSI^-$ coordinated with $Mg^{2+}$ is weakly observed due to the steric hindrance. It should be noted that the coordination structure of five O_$TFSI^-$ and one O_$N_{OX}^{+}$ coordinated with $Mg^{2+}$ is rare in all $MgTFSI_2$/ILs electrolytes, since the alkoxy-functionalized chain of $N_{OX}^{+}$ will bend and have a strong steric hindrance with the neighboring $TFSI^-$ as shown in Figure S3.

Then, the coordination number of different oxygen atoms in $N_{OX}^{+}$ around $Mg^{2+}$ is calculated and shown in Figure S4. Unpredictably, the oxygen atoms in $N_{OX}^{+}$ exhibit different coordination ability, where the O1 and terminal oxygen atoms hardly coordinate to $Mg^{2+}$ originating from the lower negative charge in comparison with internal oxygen atoms of alkoxy chain (Table S1). This is mainly due to the terminal methyl which is an electron-donating group leading to a decreasing electron density and negative charge of the bonded oxygen atom. Similarly, the quaternary ammonium group has a greater electron-accepting ability, resulting in a lower negative charge of the closer oxygen atom.[24] However, the coordination ability of oxygen atom O2 in $N_{O3}^{+}$ is insufficient to coordinate with $Mg^{2+}$ due to steric hindrance and electrostatic repulsion interaction. Therefore, the $Mg^{2+}$ first solvation shell is composed entirely of $TFSI^-$ in $MgTFSI_2/N_{O1}$TFSI and $MgTFSI_2/N_{O3}$TFSI electrolyte (Figure S5a). Conversely, there are three and five oxygen atoms with strong coordination ability, single $N_{O5}^{+}$ or $N_{O7}^{+}$ can surround and coordinate $Mg^{2+}$ to displace $TFSI^-$ in the first solvation shell (Figure S5, parts b and c). Moreover, the special coordination structure of $Mg^{2+}$ and $N_{O5}^{+}$ or $N_{O7}^{+}$ have a noticeable effect on the coordination structure of $TFSI^-$. For $MgTFSI_2/N_{O1}$TFSI and $MgTFSI_2/N_{O3}$TFSI electrolyte. $Mg^{2+}$ coordinates with $TFSI^-$ through both bidentate and monodentate geometries, corresponding to the $Mg^{2+}$−N($TFSI^-$) RDFs peaks at approximately 3.9 and 4.1 Å in Figure S6, respectively. The relative peak intensities vary considerably with ILs solvent; the peak assigned to bidentate geometry disappears in $MgTFSI_2/N_{O5}$TFSI and $MgTFSI_2/N_{O7}$TFSI electrolyte. This is likely due to the encirclement of $N_{O5}^{+}$ or $N_{O7}^{+}$ to $Mg^{2+}$, which is not conducive to the presence of bidentate geometry.

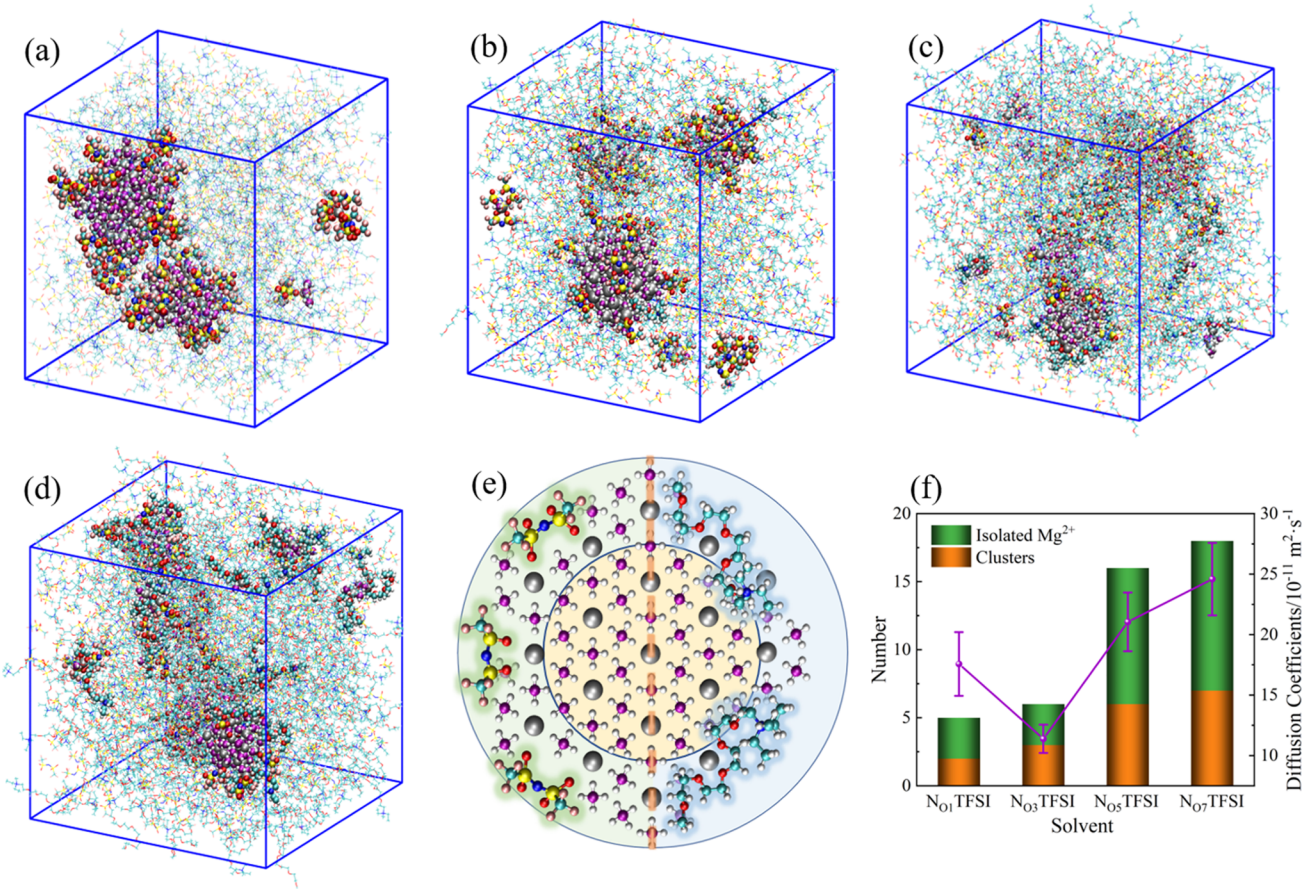


**Figure 2.** Representative simulation snapshots of (a) $Mg(BH_4)_2/N_{O1}TFSI$, (b) $Mg(BH_4)_2/N_{O3}TFSI$, (c) $Mg(BH_4)_2/N_{O5}TFSI$, and (d) $Mg(BH_4)_2/N_{O7}TFSI$ electrolyte. (e) Representative magnified simulation snapshots of the ion cluster. The purple balls represent B atoms, and other symbols are the same as those in Figure S1. (f) Diffusion coefficient (purple point) for $Mg^{2+}$ and the number of isolated $Mg^{2+}$ or clusters in $Mg(BH_4)_2$/IL electrolyte.

Parts d–f of Figure 1 show the RDF and coordination number of $Mg^{2+}$–$B(BH_4^-)$, $Mg^{2+}$–$O(TFSI^-)$, and $Mg^{2+}$–$O(N_{OX}^+)$ in $Mg(BH_4)_2$/IL electrolyte. The $Mg^{2+}$ coordination structure is completely rearranged when the $Mg^{2+}$ source is changed to $Mg(BH_4)_2$. As shown above, when $MgTFSI_2$ is dissolved in ILs, there is always $TFSI^-$ coordinated to $Mg^{2+}$ (>2). However, when the salt is $Mg(BH_4)_2$, $BH_4^-$ possesses a high coordination number with $Mg^{2+}$ and dominates the solvation shell, whereas the $TFSI^-$ is rarely coordinated to $Mg^{2+}$. The $Mg^{2+}$–$O(N_{OX}^+)$ coordination number increases in the solvent with long-chain cation, but is much smaller than in $MgTFSI_2$/IL electrolyte. The difference in ion agglomeration can be understood from the binding energies between $Mg^{2+}$ and different anions, which follows $Mg^{2+}$–$TFSI^-$ (−1237.4 kJ·mol$^{-1}$, monodentate) < $Mg^{2+}$–$BH_4^-$ (−1451.5 kJ·mol$^{-1}$) < $Mg^{2+}$–$TFSI^-$ (−1469.8 kJ·mol$^{-1}$, bidentate). The binding energy is calculated at the B3LYP/6-311++G** level of theory with basis set superposition error (BSSE) correction. A comparison of the binding energies of the $Mg^{2+}$–$TFSI^-$ through monodentate geometry and $Mg^{2+}$–$BH_4^-$ suggests that the interaction of the $BH_4^-$ with the $Mg^{2+}$ is stronger than that of the monodentate $TFSI^-$. Thus, $Mg^{2+}$ tends to coordinate with $BH_4^-$ and form clusters rather than with $TFSI^-$. In particular, the RDF of $Mg^{2+}$–$B(BH_4^-)$ displays distinct double peaks at 2.3 and 2.7 Å corresponding to the $BH_4^-$ coordinates with $Mg^{2+}$ through bidentate and monodentate geometries, which is actually the opposite of previous observations that all $BH_4^-$ coordinated with $Mg^{2+}$ through bidentate geometry.[25] Figure S7a exhibits the RDFs and coordination number of $Mg^{2+}$–$H(BH_4^-)$, a single distinct RDF peak can be identified at 1.8 Å, indicating direct and stronger coordination between $Mg^{2+}$ and $H(BH_4^-)$. Moreover, as cluster formation occurs, each $BH_4^-$ can coordinate with 2 or even 3 $Mg^{2+}$, leading to different coordination structures that are responsible for the double RDF peaks (Figure S7b).

Parts a–d of Figure 2 show the representative snapshots of the ion clusters formed by $Mg(BH_4)_2$ salts dissolved in different ILs solvent. In an effort to understand the mechanism of cluster formation, we constructed a nonexistent electrolyte $N_{O3}BH_4/N_{O3}TFSI$ to compare with $MgTFSI_2/N_{O3}TFSI$ and $Mg(BH_4)_2/N_{O3}TFSI$ electrolyte. We ascertained that the clusters are only discovered in $Mg(BH_4)_2/N_{O3}TFSI$ electrolyte (Figure S8), which suggests that both metal ions coordination center and small-sized molecules with strong coordination ability are necessary for cluster formation. Similarly, clusters were also found in $Mg(BF_4)_2$ electrolytes.[26] Several distinct differences in the clusters are observed directly from these simulation snapshots. The $Mg^{2+}$ inside the clusters are mainly coordinated with $BH_4^-$ due to the strong coordination interaction between them, and the $Mg^{2+}$ located at the cluster surface can coordinate with other components, such as $TFSI^-$ or $N_{OX}^+$ (Figure 2e). Similar to the analysis above, $TFSI^-$ coordinates with $Mg^{2+}$ located at the cluster surface in $N_{O1}TFSI$ and $N_{O3}TFSI$ solvent (Figure 2e left). Moreover,

the ease with which $N_{O5}^+$ or $N_{O7}^+$ displace $TFSI^-$ originates from the relatively weak coordination of $TFSI^-$ to $Mg^{2+}$ (Figure 2e right). As a result, the $Mg^{2+}$–$TFSI^-$ coordination number decreases significantly to 0.52 and 0.26 in $Mg(BH_4)_2$/$N_{O5}$TFSI and $Mg(BH_4)_2$/$N_{O7}$TFSI electrolyte (Figure 1e). The proportion of $Mg^{2+}$ in which zero to six coordinated oxygen atoms ($O(TFSI^-)$) can also support this conclusion (Figure S2b); there are increasing $Mg^{2+}$ that are not coordinated to $TFSI^-$ as the cation chain grows. This is more effective at enhancing the reversibility of the Mg deposition and dissolution processes.[21,26]

The diffusivity of metal ions within the electrolyte is a vital factor for battery performance. Recent studies demonstrate that ion clusters in organic electrolytes strongly influence the transport behavior of metal ions.[16,18] Therefore, we analyzed the correlation of cluster formation and $Mg^{2+}$ diffusion in $Mg(BH_4)_2$/IL electrolyte. Figure 2f shows the calculated diffusion coefficient for $Mg^{2+}$ in various electrolytes. Generally, the viscosity of ILs increases with the growth of cation chain, which in turn limits the motion of metal ions.[21,25,27] According to the simulation snapshots $Mg^{2+}$ are distributed in clusters or as an isolated $Mg^{2+}$ ($Mg^{2+}$–$Mg^{2+}$ distance greater than 5 Å). Therefore, viscosity and cluster formation can affect the $Mg^{2+}$ diffusion. When the $Mg^{2+}$ are distributed in clusters, the calculated diffusion coefficient may characterize the cluster mobility and $Mg^{2+}$ mobility within clusters. Although the $Mg^{2+}$ mobility within clusters is certainly highly correlated with electrolytes performance, the isolated $Mg^{2+}$ with faster mobility is also of intrinsic importance for electrolyte performance.[16,28] Thus, the numbers of clusters and isolated $Mg^{2+}$ are listed in Figure 2f. Due to the poor coordination ability of $N_{O1}^+$ and $N_{O3}^+$, the numbers of clusters and isolated $Mg^{2+}$ are similar in $Mg(BH_4)_2$/$N_{O1}$TFSI and $Mg(BH_4)_2$/$N_{O3}$TFSI electrolytes, which represent similar size clusters and have less effect on the diffusion coefficient. Therefore, the observed decrease of the diffusion coefficient with an increasing chain length from $N_{O1}^+$ to $N_{O3}^+$ can be attributed to the higher viscosity from the larger cations. However, ILs with long alkoxy chain cation are accompanied by unconventional larger diffusion coefficients. Moreover, increasing cation chain length induces a significant increase in both isolated $Mg^{2+}$ and clusters number. These findings are similar to those observed for $Mg(BH_4)_2$ salt dissolved in glymes G1–G4.[16] We propose a 2-fold approach to assess the cluster's influence on $Mg^{2+}$ diffusion responsible for this phenomenon: (1) more isolated $Mg^{2+}$ with faster mobility increases the calculated average diffusion coefficient; (2) the increasing cluster number implies smaller clusters based on a constant number of $Mg^{2+}$, and smaller clusters tend to carry a faster diffusion.

To verify the presence of ion clusters in $Mg(BH_4)_2$ electrolyte, small-angle X-ray scattering was carried out for $N_{O1}$TFSI and $N_{O7}$TFSI electrolyte. The widely studied *N*-butyl-*N*-methylpyrrolidinium bis(trifluoromethanesulfonyl) imide ($Pyr_{14}$TFSI) and *N*-(2-methoxyethyl)-*N*-methylpyrrolidinium bis(trifluoromethanesulfonyl) imide ($Pyr_{12O1}$TFSI) electrolytes are also examined for comparison.[21] The collected SAXS patterns are shown in Figure 3. It is immediately appreciable how the presence of the Mg salt induces an increased scattered intensity at very low $q$ values (i.e., large real distances) in all the samples except the one with the $N_{O7}^+$ cation. Such behavior is known as "Low q Excess" (LqE) in IL-based systems.[29] This peculiar phenomenon is ascribed to large-scale density fluctuations in the system, as highlighted in

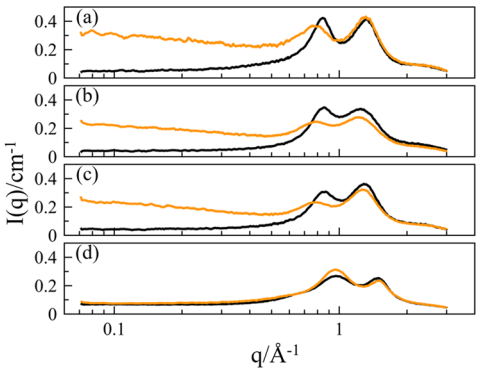


**Figure 3.** SAXS patterns for the pure ionic liquids (black) and their mixtures with $Mg(BH_4)_2$ (orange): (a) $Pyr_{14}$TFSI; (b) $N_{O1}$TFSI; (c) $Pyr_{12O1}$TFSI; (d) $N_{O7}$TFSI.

our previous works.[30−32] The driving force for the formation of such large agglomerations is the low affinity of the solute molecule toward the solvent. As a consequence, the solute molecules tend to cluster together, generating regions of high solute concentration (usually denser) floating in a solvent-rich matrix (usually less dense). The cluster size and shape distributions are generally highly dispersed, thus the SAXS pattern does not show a clear peak-like feature but rather an increased background emerging from the superposition of all the differently sized (shaped) clusters. It should be noted, though, that the mixtures appear homogeneous and perfectly transparent at the macroscopic scale. Obviously, the pronounced nanoscale heterogeneity has an evident impact on the dynamics of the system.[31,33] The solute–solvent affinity could be estimated by the intensity of the LqE, i.e., the more intense the LqE is, the lesser the affinity. In the ideal case of a perfectly homogeneous mixture, the LqE would not be observable. In the studied systems, the $Mg(BH_4)_2$ salt affinity toward the IL cations is $N_{O7}^+ \gg Pyr_{12O1}^+ \approx N_{O1}^+ > Pyr_{14}^+$, which is in line with our computational findings. The presence of a large number of oxygen atoms on the $N_{O7}^+$ cation facilitates the coordination of $Mg^{2+}$, effectively dissociating the solid salt forming solvent separated ion pairs (SSIP). The other cations either have only a small number of oxygen atoms ($Pyr_{12O1}^+$ and $N_{O1}^+$) which are less effective in coordinating the metal, or they do not have oxygen atoms at all ($Pyr_{14}^+$) therefore the cation cannot coordinate with $Mg^{2+}$.

The reductive stability of the electrolyte dictates the electrochemical performance of the battery. Ab initio dynamic simulations (AIMD) are performed to evaluate the spontaneous structure formation and the change in Gibbs free energy values ($\Delta G$) upon addition of single or two electrons to the $Mg^{2+}$-solvent complexes. Based on the above analysis regarding the ion pairs and ion clusters, the AIMD is carried out for three types of models. For the electrolyte of $Mg(TFSI)_2$ salt dissolved in ILs, the $Mg^{2+}$ first solvation shell consists of $TFSI^-$ and $N_{OX}^+$ accompanied by the formation of ion pairs. Therefore, the model I "$Mg–N_{O5}^+–(TFSI^-)_3$" was constructed to represent the $Mg(TFSI)_2$ electrolyte. When the salt is changed to $Mg(BH_4)_2$, due to the formation of ion clusters, $Mg^{2+}$ were divided into two categories located at the cluster surface and inside the cluster. The first solvation shell of $Mg^{2+}$ located at the cluster surface contains $TFSI^-$, $BH_4^-$ and $N_{OX}^+$, which is represented by model II as "$Mg–N_{O5}^+–(TFSI^-)_2–(BH_4^-)_1$". $Mg^{2+}$ inside the ion clusters only coordinates with $BH_4^-$, however, for a more intuitive

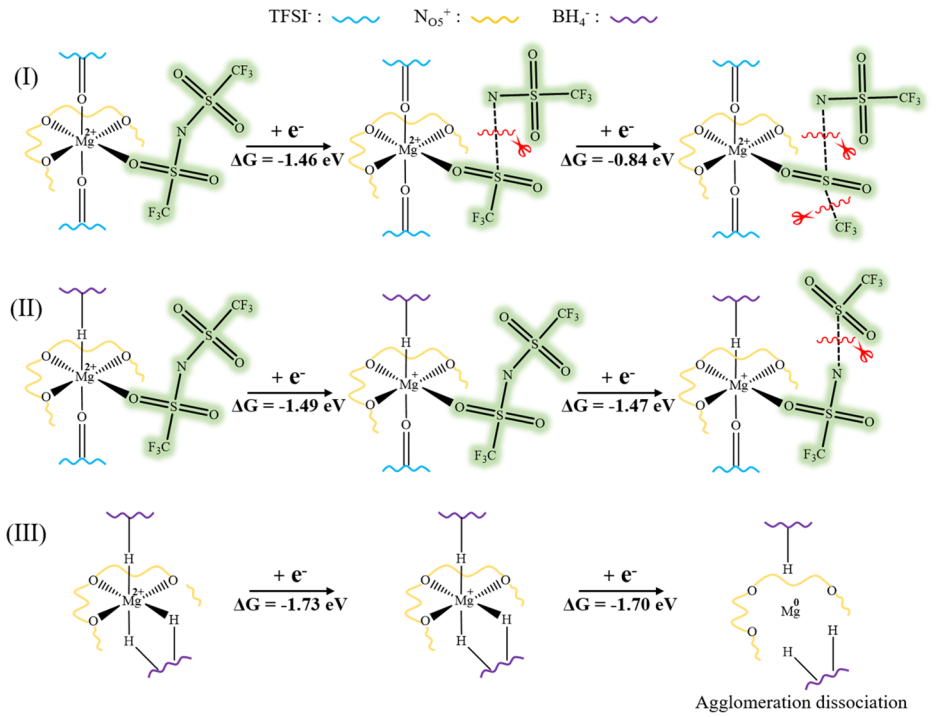


**Figure 4.** Schematic illustration of the AIMD simulation of different agglomeration for Mg deposition and dissolution processes. The change in Gibbs free energy values ($\Delta G$) upon addition of an electron to the agglomeration is also indicated in the figure.

comparison with model I and II, it is assumed that $N_{OX}^+$ and $BH_4^-$ constitute its first solvation shell, which is represented by model III as "$Mg{-}N_{O5}^+{-}(BH_4^-)_2$". The reduction processes can be directly observed from the animations of the AIMD trajectories (Videos S1, S2, and S3 for models I, II and III, respectively).

The schematic illustration of the reduction processes of different agglomeration upon addition of single or two electrons are summarized in Figure 4. The model I undergoes spontaneous degradation by cleavage of S−N bond and S−C bond of one of the three $TFSI^-$ molecules due to sequential addition of two electrons during the AIMD simulations, which is consistent with the previously reported reduction processes of the $TFSI^-$-coordinated Mg agglomeration.[21,34] In other words, the deposition does not occur due to the suppression of the $Mg^{2+}/Mg$ redox reaction. Furthermore, when the $TFSI^-$ and $BH_4^-$ are simultaneously coordinated with Mg (model II), the addition of a single electron results in the reduction of $Mg^{2+}$ to the $Mg^+$ radical cation. The injection of two electrons can also lead to $TFSI^-$ decomposing through S−N bond cleavage. On the contrary, when the $TFSI^-$ is completely expelled from $Mg^{2+}$ first solvation shell, the model III remained stable and no parasitic degradation was observed upon addition of single or two electrons for the duration of the AIMD simulation. The agglomeration dissociation proves the reduction processes of $Mg^{2+} \rightarrow Mg^+ \rightarrow Mg^0$ process and the final product is Mg deposition. The comparative analysis shows that the suppression of $TFSI^-$ coordinated with $Mg^{2+}$ is favorable to enhance Coulombic efficiency for reversible Mg deposition and dissolution, which is more susceptible to cleavage under reducing conditions compared to $N_{OX}^+$ and $BH_4^-$. Having demonstrated the cluster formation in $Mg(BH_4)_2$ electrolytes, the $BH_4^-$ with stronger coordination ability can effectively displace $TFSI^-$ from the $Mg^{2+}$ first solvation shell, while appearing to significantly enhance the Coulombic efficiency of the electrolyte. Furthermore, larger clusters with smaller specific surface areas demonstrate that relatively less Mg located at the surface also contribute to improving Coulomb efficiency. Therefore, IL solvates with long-chain $N_{OX}^+$ or large size ion clusters are both beneficial for the reversibility of the Mg deposition/dissolution process. Specifically, our previous studies have shown that the Coulombic efficiency of $Mg(BH_4)_2$ electrolyte with alkoxy-functionalized ILs is much higher than that of $Mg(BH_4)_2/Pyr_{14}TFSI$ electrolyte, while the Mg deposition/stripping process is not possible in $MgTFSI_2/Pyr_{14}TFSI$ electrolyte, which is consistent with the simulation results.[21]

In conclusion, the molecular mechanisms for the effect of ion clusters on the electrochemical and transport behavior of Mg IL-based electrolytes have been explored using MD simulations and small-angle X-ray scattering. The incorporation of $Mg^{2+}$ into clusters significantly impeded the mobility of $Mg^{2+}$ compared to the ion pairs, while diffusion is increasingly restricted with large cluster size. On the contrary, larger clusters with smaller specific surface areas contribute to improving the Coulombic efficiency. This work highlights the role of microstructural and dynamical heterogeneities in the rational design of superior multivalent electrolytes.

## AUTHOR INFORMATION


### Corresponding Authors

**Xinpei Gao** − *Key Laboratory of Ministry of Education for Advanced Materials in Tropical Island Resources, Hainan University, Haikou 570228, P. R. China*; Email: xpgao@hainanu.edu.cn

**Liqiang Zheng** − *Key Laboratory of Colloid and Interface Chemistry, Shandong University, Ministry of Education, Jinan 250100, P. R. China*; orcid.org/0000-0003-0422-9585; Email: lqzheng@sdu.edu.cn

### Authors

**Long Su** − *Key Laboratory of Colloid and Interface Chemistry, Shandong University, Ministry of Education, Jinan 250100, P. R. China*

**Alessandro Mariani** − *Helmholtz Institute Ulm (HIU), 89081 Ulm, Germany; Karlsruhe Institute of Technology (KIT), 76021 Karlsruhe, Germany*; orcid.org/0000-0002-3686-2169

**Xu Liu** − *Helmholtz Institute Ulm (HIU), 89081 Ulm, Germany; Karlsruhe Institute of Technology (KIT), 76021 Karlsruhe, Germany*; orcid.org/0000-0003-0532-316X

**Stefano Passerini** − *Helmholtz Institute Ulm (HIU), 89081 Ulm, Germany; Karlsruhe Institute of Technology (KIT), 76021 Karlsruhe, Germany*; orcid.org/0000-0002-6606-5304

**Yanan Gao** − *Key Laboratory of Ministry of Education for Advanced Materials in Tropical Island Resources, Hainan University, Haikou 570228, P. R. China*


### Notes

The authors declare no competing financial interest.

## ACKNOWLEDGMENTS


This work was supported by the National Natural Science Foundation of China (22102090, 21773141), the Natural Science Foundation of Shandong Province (ZR2019ZD45), and the Natural Science Foundation of Hainan Province (2019RC166). A.M., X.L., and S.P. acknowledge the basic funding of the Helmholtz Association.


## REFERENCES


(1) Dong, K.; Liu, X.; Dong, H.; Zhang, X.; Zhang, S. Multiscale Studies on Ionic Liquids. *Chem. Rev.* **2017**, *117*, 6636−6695.

(2) Tian, H. J.; Zhang, S. L.; Meng, Z.; He, W.; Han, W. Q. Rechargeable Aluminum/Iodine Battery Redox Chemistry in Ionic Liquid Electrolyte. *ACS Energy Lett.* **2017**, *2*, 1170−1176.

(3) Beltrop, K.; Qi, X.; Hering, T.; Roser, S.; Winter, M.; Placke, T. Enabling Bis(Fluorosulfonyl)Imide-Based Ionic Liquid Electrolytes for Application in Dual-Ion Batteries. *J. Power Sources* **2018**, *373*, 193−202.

(4) Muldoon, J.; Bucur, C. B.; Gregory, T. Quest for Nonaqueous Multivalent Secondary Batteries: Magnesium and Beyond. *Chem. Rev.* **2014**, *114*, 11683−720.

(5) Biria, S.; Pathreeker, S.; Genier, F. S.; Li, H. S.; Hosein, I. D. Plating and Stripping Calcium at Room Temperature in an Ionic-Liquid Electrolyte. *ACS Appl. Energy Mater.* **2020**, *3*, 2310−2314.

(6) Yoo, H. D.; Jokisaari, J. R.; Yu, Y. S.; Kwon, B. J.; Hu, L. H.; Kim, S.; Han, S. D.; Lopez, M.; Lapidus, S. H.; Nolis, G. M.; Ingram, B. J.; Bolotin, I.; Ahmed, S.; Klie, R. F.; Vaughey, J. T.; Fister, T. T.; Cabana, J. Intercalation of Magnesium into a Layered Vanadium Oxide with High Capacity. *ACS Energy Lett.* **2019**, *4*, 1528−1534.

(7) Canongia Lopes, J. N.; Costa Gomes, M. F.; Padua, A. A. H. Nonpolar, Polar, and Associating Solutes in Ionic Liquids. *J. Phys. Chem. B* **2006**, *110*, 16816−16818.

(8) Habasaki, J.; Ngai, K. L. Heterogeneous Dynamics of Ionic Liquids from Molecular Dynamics Simulations. *J. Chem. Phys.* **2008**, *129*, 194501.

(9) Castner, E. W.; Wishart, J. F. Spotlight on Ionic Liquids. *J. Chem. Phys.* **2010**, *132*, 120901.

(10) Araque, J. C.; Hettige, J. J.; Margulis, C. J. Modern Room Temperature Ionic Liquids, a Simple Guide to Understanding Their Structure and How It May Relate to Dynamics. *J. Phys. Chem. B* **2015**, *119*, 12727−12740.

(11) Sun, J.; O'Dell, L. A.; Armand, M.; Howlett, P. C.; Forsyth, M. Anion-Derived Solid-Electrolyte Interphase Enables Long Life Na-Ion Batteries Using Superconcentrated Ionic Liquid Electrolytes. *ACS Energy Lett.* **2021**, *6*, 2481−2490.

(12) Seo, D. M.; Borodin, O.; Han, S. D.; Boyle, P. D.; Henderson, W. A. Electrolyte Solvation and Ionic Association II. Acetonitrile-Lithium Salt Mixtures: Highly Dissociated Salts. *J. Electrochem. Soc.* **2012**, *159*, A1489−A1500.

(13) Weber, I.; Ingenmey, J.; Schnaidt, J.; Kirchner, B.; Behm, R. J. Influence of Complexing Additives on the Reversible Deposition/Dissolution of Magnesium in an Ionic Liquid. *Chemelectrochem* **2021**, *8*, 390−402.

(14) Watkins, T.; Buttry, D. A. Determination of Mg(2+) Speciation in a TFSI(−)-Based Ionic Liquid with and without Chelating Ethers Using Raman Spectroscopy. *J. Phys. Chem. B* **2015**, *119*, 7003−7014.

(15) Self, J.; Hahn, N. T.; Fong, K. D.; McClary, S. A.; Zavadil, K. R.; Persson, K. A. Ion Pairing and Redissociaton in Low-Permittivity Electrolytes for Multivalent Battery Applications. *J. Phys. Chem. Lett.* **2020**, *11*, 2046−2052.

(16) Samuel, D.; Steinhauser, C.; Smith, J. G.; Kaufman, A.; Radin, M. D.; Naruse, J.; Hiramatsu, H.; Siegel, D. J. Ion Pairing and Diffusion in Magnesium Electrolytes Based on Magnesium Borohydride. *ACS Appl. Mater. Interfaces* **2017**, *9*, 43755−43766.

(17) Drews, J.; Danner, T.; Jankowski, P.; Vegge, T.; Garcia Lastra, J. M.; Liu, R.; Zhao-Karger, Z.; Fichtner, M.; Latz, A. Modeling of Ion Agglomeration in Magnesium Electrolytes and Its Impacts on Battery Performance. *ChemSusChem* **2020**, *13*, 3599−3604.

(18) Vasudevan, V.; Wang, M.; Yuwono, J. A.; Jasieniak, J.; Birbilis, N.; Medhekar, N. V. Ion Agglomeration and Transport in $MgCl_2$-Based Electrolytes for Rechargeable Magnesium Batteries. *J. Phys. Chem. Lett.* **2019**, *10*, 7856−7862.

(19) Rajput, N. N.; Seguin, T. J.; Wood, B. M.; Qu, X.; Persson, K. A. Elucidating Solvation Structures for Rational Design of Multivalent Electrolytes-A Review. *Top Curr. Chem.* **2018**, *376*, 79−124.

(20) Hahn, N. T.; Self, J.; Han, K. S.; Murugesan, V.; Mueller, K. T.; Persson, K. A.; Zavadil, K. R. Quantifying Species Populations in Multivalent Borohydride Electrolytes. *J. Phys. Chem. B* **2021**, *125*, 3644−3652.

(21) Gao, X. P.; Mariani, A.; Jeong, S.; Liu, X.; Dou, X. W.; Ding, M.; Moretti, A.; Passerini, S. Prototype Rechargeable Magnesium Batteries Using Ionic Liquid Electrolytes. *J. Power Sources* **2019**, *423*, 52−59.

(22) Tsuzuki, S.; Shinoda, W.; Matsugami, M.; Umebayashi, Y.; Ueno, K.; Mandai, T.; Seki, S.; Dokko, K.; Watanabe, M. Structures of [Li(Glyme)](+) Complexes and Their Interactions with Anions in

Equimolar Mixtures of Glymes and Li[TFSA]: Analysis by Molecular Dynamics Simulations. *Phys. Chem. Chem. Phys.* **2015**, *17*, 126−129.
(23) Zhang, H.; Chen, F.; Lakuntza, O.; Oteo, U.; Qiao, L.; Martinez-Ibanez, M.; Zhu, H.; Carrasco, J.; Forsyth, M.; Armand, M. Suppressed Mobility of Negative Charges in Polymer Electrolytes with an Ether-Functionalized Anion. *Angew. Chem., Int. Ed.* **2019**, *58*, 12070−12075.
(24) Shimizu, M.; Yamaguchi, K.; Usui, H.; Ieuji, N.; Yamashita, T.; Komura, T.; Domi, Y.; Nokami, T.; Itoh, T.; Sakaguchi, H. Piperidinium-Based Ionic Liquids as an Electrolyte Solvent for Li-Ion Batteries: Effect of Number and Position of Oxygen Atom in Cation Side Chain on Electrolyte Property. *J. Electrochem. Soc.* **2020**, *167*, 070516.
(25) Watkins, T.; Kumar, A.; Buttry, D. A. Designer Ionic Liquids for Reversible Electrochemical Deposition/Dissolution of Magnesium. *J. Am. Chem. Soc.* **2016**, *138*, 641−650.
(26) Rajput, N. N.; Qu, X.; Sa, N.; Burrell, A. K.; Persson, K. A. The Coupling between Stability and Ion Pair Formation in Magnesium Electrolytes from First-Principles Quantum Mechanics and Classical Molecular Dynamics. *J. Am. Chem. Soc.* **2015**, *137*, 3411−3420.
(27) von Zamory, J.; Giffin, G. A.; Jeremias, S.; Castiglione, F.; Mele, A.; Paillard, E.; Passerini, S. Influence of Oligo(Ethylene Oxide) Substituents on Pyrrolidinium-Based Ionic Liquid Properties, Li(+) Solvation and Transport. *Phys. Chem. Chem. Phys.* **2016**, *18*, 21539−21547.
(28) Brinkkötter, M.; Mariani, A.; Jeong, S.; Passerini, S.; Schönhoff, M. Ionic Liquid in Li Salt Electrolyte: Modifying the $Li^+$ Transport Mechanism by Coordination to an Asymmetric Anion. *Adv. Energy Sustain. Res.* **2021**, *2*, 2000078.
(29) Mariani, A.; Caminiti, R.; Ramondo, F.; Salvitti, G.; Mocci, F.; Gontrani, L. Inhomogeneity in Ethylammonium Nitrate-Acetonitrile Binary Mixtures: The Highest "Low Q Excess" Reported to Date. *J. Phys. Chem. Lett.* **2017**, *8*, 3512−3522.
(30) Mariani, A.; Dattani, R.; Caminiti, R.; Gontrani, L. Nanoscale Density Fluctuations in Ionic Liquid Binary Mixtures with Non-amphiphilic Compounds: First Experimental Evidence. *J. Phys. Chem. B* **2016**, *120*, 10540−10546.
(31) Campetella, M.; Mariani, A.; Sadun, C.; Wu, B.; Castner, E. W., Jr.; Gontrani, L. Structure and Dynamics of Propylammonium Nitrate-Acetonitrile Mixtures: An Intricate Multi-Scale System Probed with Experimental and Theoretical Techniques. *J. Chem. Phys.* **2018**, *148*, 134507.
(32) Mariani, A.; Bonomo, M.; Passerini, S. Statistic-Driven Proton Transfer Affecting Nanoscopic Organization in an Ethylammonium Nitrate Ionic Liquid and 1,4-Diaminobutane Binary Mixture: A Steamy Pizza Model. *Symmetry* **2019**, *11*, 1425.
(33) Mariani, A.; Bonomo, M.; Wu, B.; Centrella, B.; Dini, D.; Castner, E. W.; Gontrani, L. Intriguing Transport Dynamics of Ethylammonium Nitrate-Acetonitrile Binary Mixtures Arising from Nano-Inhomogeneity. *Phys. Chem. Chem. Phys.* **2017**, *19*, 27212−27220.
(34) Gao, X. P.; Liu, X.; Mariani, A.; Elia, G. A.; Lechner, M.; Streb, C.; Passerini, S. Alkoxy-Functionalized Ionic Liquid Electrolytes: Understanding Ionic Coordination of Calcium Ion Speciation for the Rational Design of Calcium Electrolytes. *Energy Environ. Sci.* **2020**, *13*, 2559−2569.